J Mater Sci: Mater Med (2011) 22:1161–1169
DOI 10.1007/s10856-011-4286-7

Two steps bulk-surface functionalization of nanoporous alumina by methyl and vinyl-silane adsorption. Evidence for oxide surface highly reactive sites creation

Christophe Azevedo · Pierre Cenedese · Pierre Dubot

Received: 23 March 2010 / Accepted: 8 March 2011 / Published online: 2 April 2011

Abstract Functionalization of a novel nanoporous monolithic alumina synthesized from amalgam is investigated. The structure is studied by X-ray diffraction, BET, MEB and IR spectroscopy, before and after chemical functionalization by trimethylethoxy silane adsorption and annealing at high temperature. These treatments retain both monolith microstructure and nanostructure while strongly improving material mechanical properties. Allyldimethoxysilane and alcohol adsorption on the annealed samples, proves that highly reactive sites are available for further polymer grafting, as demonstrated by a significant shift of allyldimethoxysilane ν_{SiH} to 2,215 cm^{-1} and adsorbed acetate formation. Simple quantum computations on model systems support this conclusion. Chemical processes reported in this paper, allow a nanostructured alumina monoliths functionalization to optimize ceramics-polymer bonds, and to tune new hybrid biomaterial properties.

1 Introduction

Porous nanoscale materials have been widely studied in the past few years. Their applications and novel properties for catalysis reactions [1–6], medicinal treatments (cells or drugs storage and release) [7, 8], biomaterials [9–13] like hybrid polymer-ceramic or functional cement, molecular trap for environmental cleaning (air or water), sensors [14–17], electronic or magnetic devices [18], confined chemistry [19], make nanostructured-structured and nanostructured-scaled materials challenging for numerous future applications.

In this work, we report results on adsorption properties of new porous nanostructured-structured alumina monoliths. Porous monoliths consisting of nanostructured-fibrils can be obtained by a novel synthesis method [20]. Very low density (2,000 g m^{-3}) alumina hydroxides are obtained by active oxidation of aluminum in a humid atmosphere as described by Vignes [20]. These high porosity and high surface area (300 m^2 g^{-1}) ceramics present peculiar surface structures and reactive sites owing to strong curvature effects in confined space, mimicking in some ways typical zeolites and related materials properties. Thermal treatments and molecular functionalization allow to modify the chemical nature and the adsorption ability of reactive sites. These make such materials tunable for selected application, and more specifically for composite material in biomedical replacement compounds like bones complement. In the case of polymer-ceramic composite materials, interfacial bonding between oxide particles and polymer groups is of prime importance. Anchoring is realized through functionalized silane coupling agent which reacts with surface hydroxyls [21] that play a crucial role in reactivity and have a wide range of chemical activity depending on their connectivity [22–28].

For applications in which a polymer contains a polymerizable vinyl function, AllylDiMethoxySilane (ADMS) can be used as a linker molecule.

Here, we study nanoporous monoliths functionalization in two steps. The first stage is realized by exposing

C. Azevedo
College d'Odontologie Garanciere Universite Denis Diderot,
5 rue de Garanciere, 75006 Paris, France
e-mail: cazevedo@yahoo.com

P. Cenedese · P. Dubot (✉)
MCMC-ICMPE-CNRS, 2 rue Henri Dunant,
94320 Thiais, France
e-mail: pcenedese@glvt-cnrs.fr

P. Cenedese
e-mail: pcenedese@glvt-cnrs.fr

monoliths to trimethylethoxy silane (TMES) vapor followed by sample heating at 1,573 K that allows Si incorporation in the alumina network (mullite like compound). X-ray diffraction spectra and BET measurements were performed to determine samples crystallinity and porosity respectively. This first stage allows monolith structure modification while retaining nanostructure and microstructure, leading to material enhanced mechanical properties. The second functionalization stage consists of ADMS adsorption at room temperature that leads to allyl function grafting on monolith surface. Silane-surface interaction leads to ADMS hydrolysis resulting in primary alcohol formation that can also reacts with monolith surface. In order to get a better understanding on the nature of the adsorbed species, we studied by infrared spectroscopy (IR) ADMS and ethanol adsorption. Both molecule in their adsorbed state show particular behavior linked to the existence of very reactive surface sites.

We have organized our study as follows: we first describe the nanostructured monoliths processes and present the physical properties of our samples as function of thermal and chemical treatments. In a Sect. 2, we concentrate on molecules adsorption experiments investigated by transmission IR spectroscopy. Finally, we compare our results to available experimental data and/or related studies to conclude on reactive sites properties of nano-structured monoliths and the potentiality to get strongly adsorbed functionalizing species.

2 Study context

2.1 Materials and methods

2.1.1 Synthesis of porous alumina

The oxidation of pure aluminium at room temperature cannot progress because a passive layer of alumina protects the metal from the oxidation process. Wislicenus [29] observed 100 years ago that when aluminium plates or wires are amalgamated, filaments of aluminium hydroxide rapidly grow from the metal surface. The composition and the structure of these hydrated alumina filaments were described by Pinnel and Bennett [30]. Their diameter is about some nanometers and their structure is amorphous. Recently, Vignes [20] developed a new process to produce shaped alumina monoliths instead of isolated fibers.

To prepare the alumina block the following method was used. After removing the natural oxide layer on the surface of pure (99.99%) aluminium plates, a surface treatment by mercury compounds was carried out. For given temperature and hydrometric conditions, the hydration process produces the regular growth of monoliths perpendicular to the surface, provided the amount of impurities of the aluminium precursor is small. An impregnation treatment of as-prepared materials with TMES vapor at room temperature during 4 h was done. Porous alumina samples were exposed to TMES up to saturation thus achieving a complete surface reaction. Before any thermal treatment, the samples were placed in an oven for 1 h at 373 K under 10^{-1} mbar to eliminate weakly adsorbed residual molecules. Those samples were then subjected to more stringent thermal treatment for 8 h at 773 or 1,273 K. Heating the samples to 1,573 K allows Si diffusion into the monolith leading to mullite phase formation.

2.1.2 Porous alumina characterization

X-ray diffraction studies were performed using a Philips PW 1830 diffractometer equipped with a cobalt anticathode. Scans were recorded between 15 and 90 with a step of 0.025 and an acquisition time of 2 s.

Specific surfaces measurements refer to the adsorption of N_2 at 77 K. B.E.T model has been used to measure the specific surface and to estimate sample porosity. Information was extracted from isotherm in the region corresponding to relative pressures between 0.05 and 0.35 bar, involved in the formation of N_2 monolayer on the surface. IR was used to characterize monoliths and adsorbed molecules vibrational modes. A Nicolet Nexus IRTF spectrometer equipped with a MCT detector was used. In this study, wavenumbers ranging from 650 to 4,000 cm^{-1} were selected. The analysis of potential changes in the chemistry and structure of the different materials was performed using the low (delocalized phonons modes) and medium IR wavenumbers. Spectra were obtained by averaging 128 scans with a resolution of 4 cm^{-1}. The first step was to analyze the as-prepared materials, as well as the samples that were heated and/or chemically treated with TMES.

2.2 Results

2.2.1 Material structure analysis

The composition of the monolith is close to $Al_2O_3{\cdot}4H_2O$. The alumina blocks are ultra-light with a density ranging from 2 to 5 $\times$ 10^3 g m^{-3} depending on the growth conditions. They have an open porosity of 99%. The high H_2O content can be seen in Fig. 1 for E_{300}, E_{773} and E_{1273} samples (monoliths without heating treatment, heated at 773 and 1,273 K respectively). IR spectra clearly show a broad absorption band of adsorbed water stretching mode in the 3,000–3,700 cm^{-1} spectral range. For heated samples, water is re-adsorbed after cooling as shown by the broad absorption band which shape depends on annealing temperature, thus adsorbed water must have properties that

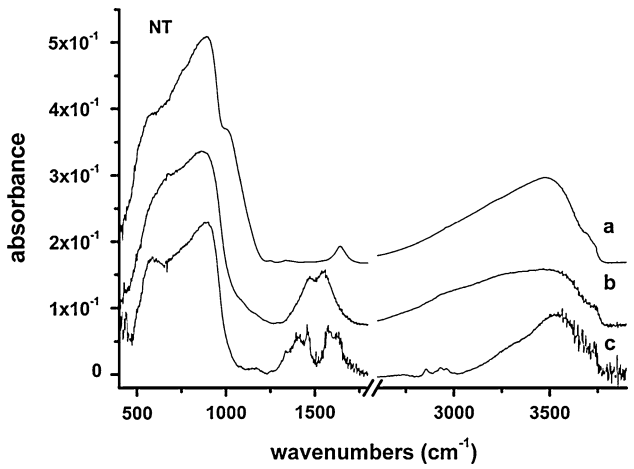

Fig. 1 IR transmission spectra of E_{300} (**a**), E_{773} (**b**) and E_{1273} (**c**) under a residual vacuum of 10^{-2} mbar. AlO phonons are in the range 500–1,100 cm^{-1}, carbonate stretching around 1,500 cm^{-1} close to the water deformation mode. The high frequency domain is related to OH stretchings

reflect monoliths surface structure. We also see that monoliths annealing leads to adsorbed carbonates (1,300–1,600 cm^{-1}). Like water, adsorbed carbonates, through their vibrational fingerprint, show that surface structure has been modified by thermal treatment.

There are two kinds of porosity in the monoliths. The micrometrical length scale corresponds to channels in the monolith's growth direction (Fig. 2) and the nano-structured-metrical length scale corresponds to channels (Fig. 3).

The diameter of the nanostructured-fibers of alumina is about 10 nm. The raw monoliths that are very brittle need to be consolidated by heating. From room temperature to 673 K, the monolith looses water and at 773 K the dehydration is nearly completed. The monoliths amorphous up to 1,143 K (Fig. 4) retain their shape and microstructure. At 1,143 K, filaments crystallize into γ-alumina and after heating at 1,273 K the crystallites of γ-alumina have an average size about 10 nm. Around 1,423 K, the transformation into α-alumina occurs and at 1,473 K α-alumina appears with grains size of about 200–300 nm.

Heating induces densification. Up to 1,373 K, i.e. in the amorphous or γ domain, the density remains very low. At higher temperature, the density increases in two steps. One order of magnitude is gained at the γ or γ–α transition [31] around 1,473 K and proceed above 1,623 K by sintering of α alumina. Nevertheless, even after heating at 1,773 or 1,873 K, aluminas with an open porosity higher than 30% are still obtained. After these thermal treatments, the overall monolith shape is maintained, despite a significant linear shrinkage goes with density increase. The fibrous microstructure of the amorphous material is transformed after crystallization, phase transitions and sintering, into strings of small grains with a limited number of connections.

High values of specific surface are measured by the B.E.T. method. They range between 300 and 420 $m^2\ g^{-1}$ depending on the monolith density. The very high porosity of starting hydrated raw monoliths allows a rapid

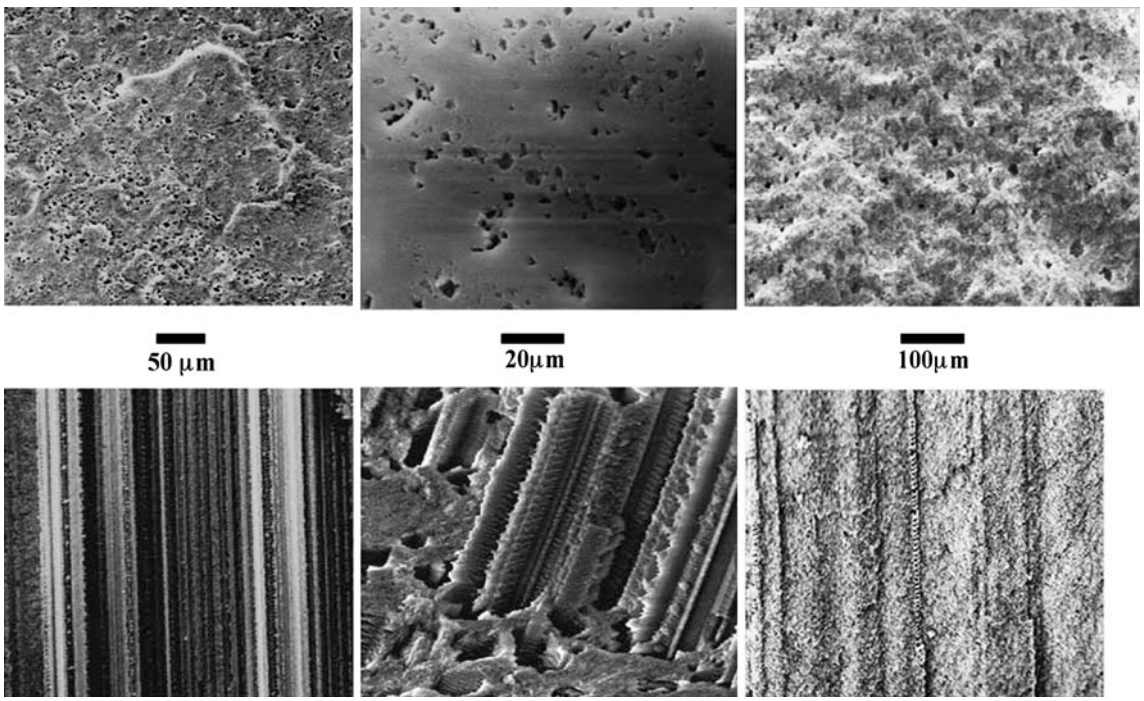

Fig. 2 Scanning Electron Microscope pictures of monoliths macroporosity for samples heated at 773, 1273 and 1573 K from the left to the right

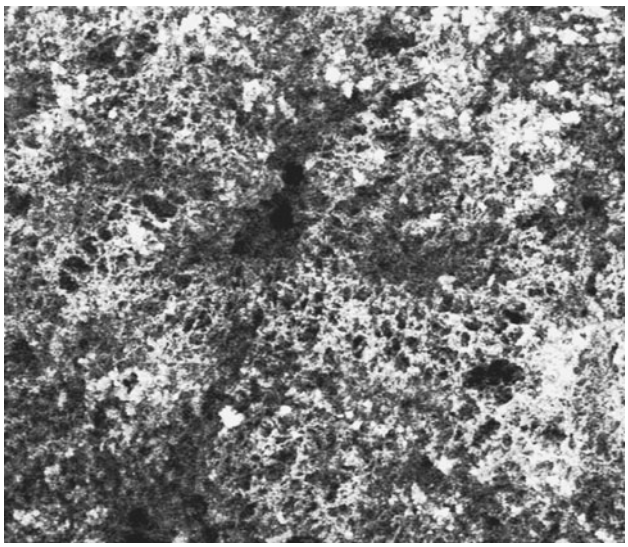

Fig. 3 SEM pictures of monoliths microporosity for samples heated at 773 K picture size is 1 μm^2

homogeneous impregnation by gaseous species. In particular, a flow of silicon alkoxides diffusing inside the porous network is hydrolyzed by the hydrated alumina surface. A remarkable modification of the thermal behavior of alumina is obtained when a low amount of silica (about 6% weight SiO_2) is incorporated by this way using TMES. Without Si addition, the specific surface area of the raw material ranges between 300 and 400 $m^2\ g^{-1}$ depending on preparative conditions. After crystallization, the specific surface area remains relatively high (around 100 $m^2\ g^{-1}$) but considerably decreases towards 5 $m^2\ g^{-1}$ at the γ–α transformation. Silica addition delays the transformation into α-Al_2O_3 up to 1,673 K instead of 1,473 K. This chemical addition stabilizes aluminas with high specific surface area at higher temperature.

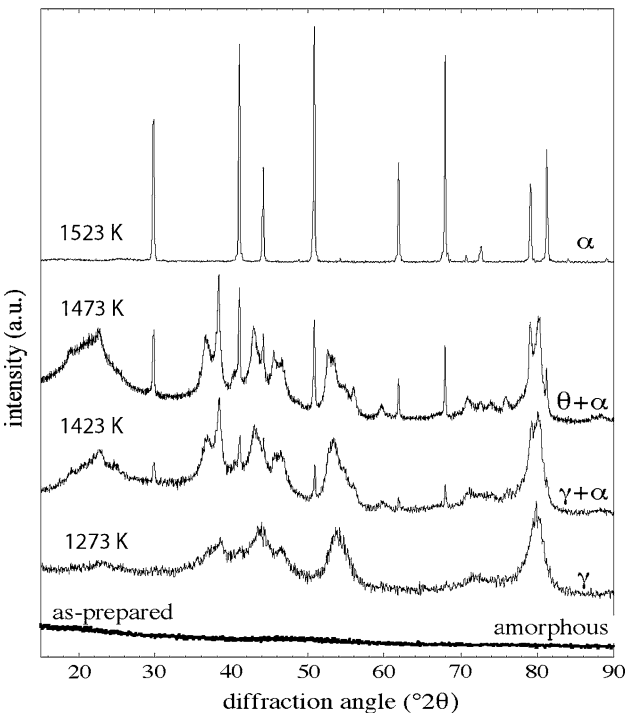

Fig. 4 X-ray diffraction spectra of bare alumina monoliths heated up to 1,523 K

2.2.2 *ADMS and ethanol adsorption: monoliths without TMES treatment*

The samples were fixed on a stainless grid and then pumped under 1×10^{-2} mbar during 30 min. The ethanol and the ADMS were introduced into the analysis chamber under a pressure of 1 mbar. The IR spectra were recorded after residual vacuum decreases to 1×10^{-2} mbar.

2.2.2.1 Ethanol adsorption IR spectra for CH_3CH_2OH interaction are shown on Fig. 5. On the contrary to E_{300}, Fig. 5 shows alcohol adsorption on E_{773} and E_{1273} as positive absorption peaks emphasizes ethoxy species formation, correlated to hydroxyls consumption (negative peak at 3,737 cm^{-1}). Referenced to the free molecule, the ν_{CO} stretching mode for E_{773} is blue shifted to 1,105 cm^{-1} while the CH stretching modes are red shifted to 2,945 and 2,826 cm^{-1}.

For E_{1273}, two ν_{CO} peaks located at 1,105 and 1,059 cm^{-1} refer to two distinct reactive sites. We remark that OH surface are no longer implied in the adsorption process. We also note that the ν_{CH} broad band differs between E_{773} and E_{1273}. The inset of Fig. 5 zooms this spectral domain and a main peak at 2,976 cm^{-1} is observed

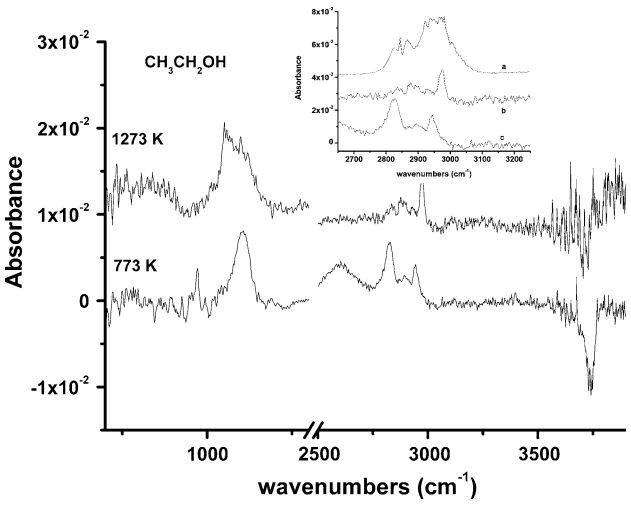

Fig. 5 IR spectra for bare samples in the case of ethanol adsorption: E_{1273} and E_{773}. Positive peaks show that ethanol adsorbs on the monolith. Negative peaks corresponds to consumption of surface hydroxyls during ethoxy formation. The *inset* zooms the CH stretchings domain for the free molecule (*a*), E_{1273} (*b*) and E_{773} (*c*)

for E_{1273} while for E_{773} two major peaks point at 2,837 and 2,930 cm^{-1}.

In summary, ethanol adsorption on raw samples (free from TMES treatment), reveals a differential reactivity. In heated samples, free OH groups disappear and lead to new reactive sites where the alcohol C–OH function is transformed to CO^- alcoholate group.

2.2.2.2 ADMS adsorption Electron transfer between the adsorbed molecule and the surface ($Al^{\delta+}$) sites modifies the ADMS–SiO bond and by the way influences electrons sharing on the SiH group. The ν_{SiH} stretching that is around 2,140 cm^{-1} for the isolated molecule, is sensitive to such a perturbation and frequency shifts are expected as function of surface cations environment and local charge.

IR spectra after ADMS interaction are shown on Fig. 6. Spectra present similarities, namely the appearance of silane peaks (ν_{CH}, ν_{SiO}, $\nu_{C=C}$, ν_{SiH}) and the removing of hydroxyls. In fact, two kinds of surface OH disappear at frequencies 3,740 and 3,700 cm^{-1} during chemisorption. The second peak is weaker and appears as a shoulder of the main peak making the absorption band asymmetric. This observation confirms the role of surface hydroxyls in the anchoring of silanes on the oxide surface.

ADMS vinyl function is highlighted by the ν_{CH} stretching modes at 3,087 cm^{-1} (majority peak) and 3,070 cm^{-1}. This splitting results from two distinct adsorption sites as confirmed by the folding of the absorption band ν_{SiH} at 2,170 and 2,130 cm^{-1} shown on the leftmost inset of Fig. 6.

For these doublets, low frequency peaks are associated to the same adsorbed species (E1: 3,087 cm^{-1} with 2,170 cm^{-1}, E2: 3,070 cm^{-1} with 2,130 cm^{-1}). Comparing these values, we deduce that the ADSM is bonded to a surface cation of stronger coordination [30] for the adsorbed specie E2, as discussed later. This conclusion is also attested by the splitting of the vinyl $\nu_{C=C}$ towards 1,600 cm^{-1} with bands at 1,637 cm^{-1} and at 1,580 cm^{-1}.

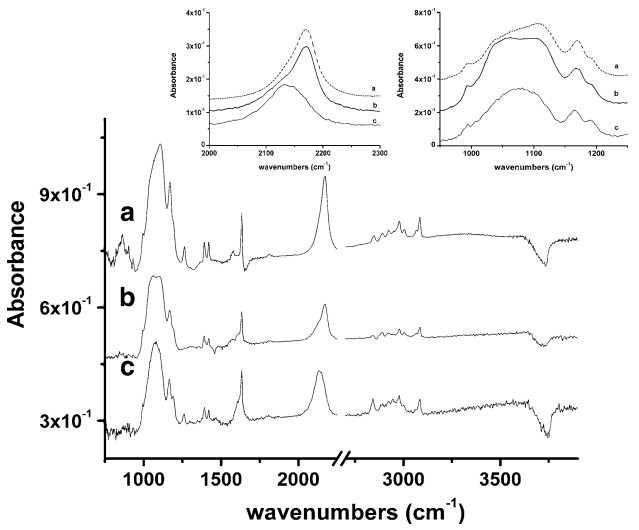

Fig. 6 IR spectra for ADMS adsorption onto E_{300} (*a*), E_{1273} (*b*) and E_{773} (*c*). The *leftmost inset* zooms the ν_{SiH} range and the rightmost refers to low frequency domain

Around 1,000 cm^{-1}, the spectra are relatively similar. For the E_{300} sample, a broad band is composed of the peaks: 1190, 1174, 1110, 1063, 1040, 990, 862 and 1580 cm^{-1}. These frequencies correspond Si–O and Al–O (towards 1,200 cm^{-1}, 1006 and 872 cm^{-1}) vibrations while the frequency at 1,100–1,040 cm^{-1} signals an ethoxy adsorption. This confirms the mechanism of hydrolysis of the ADMS Si–O–C bond and the formation of an ethanol molecule.

The comparison of E_{300}, E_{773} and E_{1273} IR spectra confirms the presence of two different reactive sites for silane adsorption. These spectra however present significant differences in the low frequencies range as it is shown in the rightmost inset of Fig. 6 where a broad absorption band seems made up of a triplet located near 1040, 1060 and 1105 cm^{-1} with different weights.

For E_{1273}, the absorption band located at 1,040 cm^{-1} seems more important than for E_{773}, corroborating the adsorption of an ethoxy and thus enforces results obtained with ethanol. For E_{300} we observe a band in this range oppositely to the experiment with ethanol. ADMS adsorption shows differential reactivity as function of the sample annealing and confirms crystallographic differences observed in X-ray. The nature of the adsorbed species seems complex and a competitive adsorption between silane and ethoxy clearly appears.

The samples E_{300} and E_{1273} behave similarly with respect to ADMS (low frequency, SiH and OH), whereas E_{773} lets appear some differences.

2.2.3 *ADMS and ethanol adsorption: monoliths with TMES treatment*

The goal of the TMES treatment is to promote the appearance of $Si^{\delta+}$ cations during the formation of the SiAlO (standard mullite) mixed oxide. Silicon addition onto the surface should modify the monolith reactivity as the silicon oxide is known to be very covalent with a weak local charge [32]: δ^+ about 1.30 e. Then we can expect different sites for molecule anchoring.

We present on the Fig. 7 the IR spectrum of the powder treated with the TMES then heated up to 1,573 K (E_{TMES}) to be compared with untreated E_{1273}. The formation of mixed oxide is evidenced by the peak at 1,170 cm^{-1} that is usually observed in aluminosilicates [33–38].

2.2.3.1 Ethanol adsorption Figure 8c displays the IR spectrum obtained after CH_3CH_2OH interaction. We see a weak CO band at 1,050 cm^{-1}, while the spectrum is

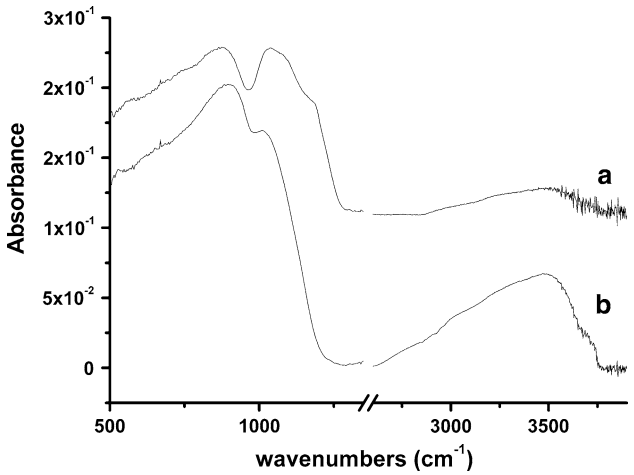

Fig. 7 IR spectra for E_{TMES} (*a*) and E_{1273} (*b*)

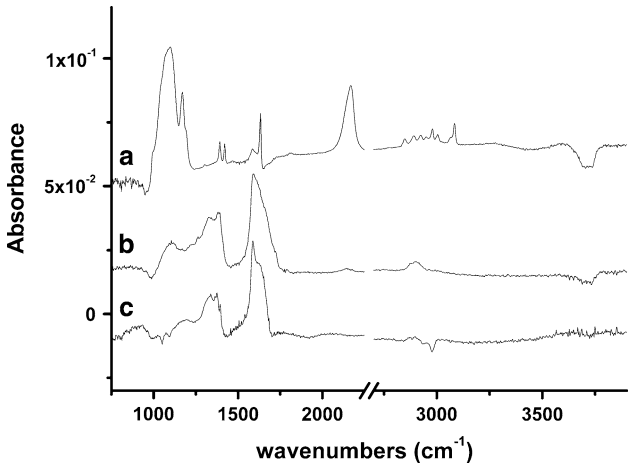

Fig. 8 IR spectra for different probe molecules on E_{TMES}: (*a*) ADMS, (*b*) ethanoic acid, (*c*) ethanol

dominated by carboxylate absorption peaks near 1632, 1592, 1378 and 1325 cm^{-1}. This spectrum can be compared with the one of ethanoic acid shown in Fig. 8b.

From these observations, we suggest that the alcohol adsorption, through alcohol deprotonation by reaction with $Si^{\delta+}$ sites, leads to carboxylate-like adsorbed specie even at room temperature.

2.2.3.2 ADMS adsorption On Fig. 8a, we observe that the ADMS adsorbs. Referring to the raw sample, we observe light shifts of OH and Si–H stretching modes. For ν_{OH}, we notice the loss of at least two kinds of hydroxyls. For the bare sample, the interaction with the ADMS revealed a broad and negative peak composed of two components at 3,730 and 3,690 cm^{-1}. The E_{TMES} exposed to ADMS now presents two negative peaks at 3,745 and 3,680 cm^{-1}. These spectral differences correspond to modification of surface OH properties owing to TMES and annealing treatment. In spite of these transformation, we notice that samples are still able to anchor silane. In addition, this difference of reactive sites is highlighted by the ν_{SiH} which also shows two absorption bands. For the bare sample, ADMS adsorption had a positive peak made of two components at 2,170 and 2,130 cm^{-1}, whereas for E_{TMES}, the positive peak components points now at 2,175 and 2,215 cm^{-1}.

3 Discussion

When the ethanol dissociates on oxides to form a surface ethoxy, ν_{CO} is blue shifted, the CO bond being reinforced by charge transfer from the surface. The ionicity of CO^{-} bond drives the strength of the shift. In contrast, binding with metallic atoms produces a red shift [39]. In the case of a similar molecule like methanol, adsorption on divided oxides [40–44] leads to monodentate, bidentate and tridentate species for which the ν_{CO} is respectively in the spectral ranges 1013−1047, 1073−1092 and 1104−1124 cm^{-1}. However, in complex oxide surface structure where defective ions are ill coordinated, these attributions can significantly deviate, as Local Density Of States can be strongly affected [45]. For E_{773}, one ν_{CO} peak around 1,105 cm^{-1} have clearly been identified while for E_{1273}, two ν_{CO} peaks at 1,105 and 1,059 cm^{-1} have been associated with two distinct adsorbed ethoxy. These values are greater than the free molecule frequency at 1,050 cm^{-1} and indicates a CO bond reinforcement for the adsorbed ethoxy.

In the same vain, the free molecular frequencies of ethyl CH group at 2844, 2938 and 2974 cm^{-1} are red shifted upon formation of ethoxy (2800, 2880 and 2932 cm^{-1}). We noticed that the ν_{CH} band change of shape for adsorbed states E_{773} and E_{1273}. In particular we observed that the intensity of the peak corresponding to the $\nu^{as}_{CH_2}$ strongly fell for E_{1273} compared with E_{773}, and affects the two molecular species identified by the CO band doublet.

To interpret the above observations, we now evaluate from simple NDDO [46] quantum computations the $\nu^{as}_{CH_2}$ susceptibility to charge transfer towards the ethoxy oxygen atom. We consider a model system where charge transfer between O and the aliphatic chain is variable. In this model the H atom of the ethanol hydroxyl group is substituted by organic groups of different inductive effects. The results quoted in Table 1 show that the transfer of electron towards oxygen is correlated to the strength of the dipolar momentum or intensity. Although the calculated frequencies are precise only to a few tenth of cm^{-1}, trends are highly physical.

Table 1 Computed $v^{as}_{CH_2}$ intensity for different ethanol like molecules where the terminal H is substituted by groups having variable inductive properties

Molecule	$v^{as}_{CH_2} T_{Dipole}$
CH_3CH_2OH	0.40
$CH_3CH_2OCH_3$	0.33
$CH_3CH_2O^-$	0.13
$CH_3CH_2OCF_3$	0.01
$CH_3CH_2OC_2F_5$	0.05

Therefore, for E_{1273}, we conclude that monolith surface has a greater capacity to attract the electrons of the adsorbed molecule irrespectively to the adsorption site. This effect can be related to a modification of the electronic structure of the aluminum oxide with annealing, as the HOMO–LUMO separation (gap between the valence and the conduction band) drives the electron transfer toward the molecule [47]. Remark that for E_{773} and E_{1273}, an ethoxy species with v_{CO} at 1,105 cm^{-1} is present in both case even if surface charge transfer is different as shown by the v_{CH_2} intensity. We conclude that surface bonding informations drawn from v_{CO} shift and v_{CH_2} intensity are not necessarily coupled. For E_{1273}, compared to the E_{773}, we found a greater molecule-surface charge transfer for the two different kind of ethoxy species revealed by v_{CO} at 1,105 and 1,060 cm^{-1}. Thus, regardless to the v_{CO} shift, the ethoxy are more strongly adsorbed in relation to the appearance of stronger reactive sites following annealing at higher temperature.

Whereas the surface OH disappeared when E_{773} was exposed to ethanol, they clearly do not participate in the adsorption process for E_{1273}. This is an evidence that surface hydroxyls of greater basicity has been removed during annealing at 1,273 K, associated with the formation of aluminum surface cations of increased reactivity.

For E_{TMES}, the formation of carboxylate following the interaction of ethanol have already been observed on some kind of oxides [48] generally after annealing at 340 K. This highlights the very particular reactional properties of this sample as it is necessary that strong nucleophilic entities like $O^{\delta-}$ are in the vicinity of the R-CO^- adsorption site to attack the $C^{\delta+}$ atom. This might appear paradoxical since we introduced more covalent Si–O bonds on the surface. Qualitatively, the structural addition of a cation with a different electronegativity, silicon instead of aluminum, modifies the Al–O and Si–O bonds iono-covalency with respect to pure oxides, and thus affects the local cationic charges. Silicon addition, whose oxide is more covalent than aluminum oxide, makes the bonds Al–O more ionic in the mixed oxide and thus increases the oxygen ions charge [32, 49]. The ion $O^{\delta-}$ being more charged, it is more electrophile to attack the C of the adsorbed ethoxy.

For E_{TMES} as for the sample E_{1273} we observed that OH were not invoked in the ethoxy formation. This means that like annealing at 1,273 K, TMES treatment removes the basic surface OH, but does not prevent alcohol to react with monolith surface.

The ADMS adsorption on raw and TMES treated samples led to the silane grafting and surface OH consumption. This results from ADMS hydrolysis leading to silanol and ethanol production [21]. Firstly, we show in Fig. 6 that alcoholate is clearly adsorbed on each samples as revealed by the v_{CO} near 1,050 cm^{-1}. Particularly, on the E_{300}, we observed this adsorption while it was not effective in the case of ethanol interaction. We interpret it either as a production of ethoxy during ADMS hydrolysis, specie that is much more reactive than ethanol, or either as an energy contribution from ADMS hydrolysis to the ethanol adsorption. The ethoxy adsorption during silane grafting leads to a decrease of the anchored silane density as both molecules compete to react with the surface, and is thus baneful for monolith functionalization.

The v_{SiH} absorption band proved to be a good marker for adsorption sites strength. In order to quantify v_{SiH} susceptibility with respect to electron density, we have computed v_{SiH} for different ADMS like molecules where variable number of methyl hydrogen atoms have been replaced by fluorine.

As the number nF of fluorine atoms increases, electrons withdrawn from Si flow to the CF_{nF} group. This quantum computation qualitatively demonstrates that v_{SiH} decreases as nF increases as shown on Fig. 9. This calculation shows that v_{SiH} can be use as a good probe to characterize the electron transfer between the grafted silane molecule and the surface.

Therefore, for raw samples, we identify by ADMS adsorption, two kinds of surface sites at v_{SiH} at 2,130 and

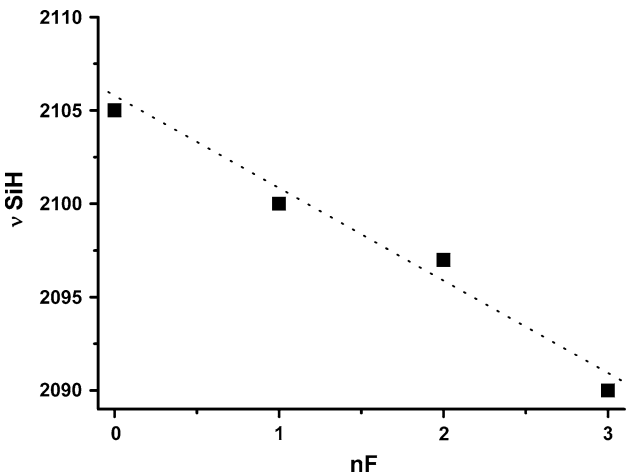

Fig. 9 Computed v_{SiH} stretching for ADMS like molecules where variable number (nF) of methyl H atoms have been replaced by F

2,170 cm^{-1}. These two values border ν_{SiH} of the free molecule (2,140 cm^{-1}). For E_{TMES}, two peaks appear at higher frequency (2,175 and 2,215 cm^{-1}). The highest frequency band is associated with molecules adsorbed on a surface silicon cation as it could be emphasized from Fig. 9. Indeed the degree of covalency being more important in the bond Si–O, the charge transferable from the Si cation towards the silane molecule is higher for silicon than for aluminium. This also implies a stronger chemical bond between the ADMS and the surface of the TMES treated monoliths.

4 Conclusion

A new nanoporous monolithic alumina was synthesized starting from amalgam. Chemical treatment by TMES and annealing allowed to modify the crystallographic structure of the monoliths while preserving both microstructure and nanostructure. This modification of structure, observable from X-ray and the IR low frequency modes, is linked to the appearance of reactive surface sites distribution changes.

The adsorption ADMS and ethanol molecules on these samples shows the presence of highly reactive sites allowing strong binding to the surface. In particular, the maximum shift of the mode ν_{SiH} to 2,230 cm^{-1} of the adsorbed ADMS, is a marker of this increased reactivity and stronger interfacial bonds. A simple quantum calculation relative to the ν_{SiH} susceptibility, qualitatively attests an important electronic transfer from the surface towards the molecule when the temperature of the heat treatment increases or when surface is treated with TMES.

We observed as a function of surface states, a modification of the frequency of hydroxyls implied in the ADMS grafting.

This study confirms the interest of the functionalization to control surface reactivity in order to optimize ceramics-polymer bonds, and more specifically to design new hybrid biomaterials for bones complement.

References

1. Kirchner A, MacKenzie KJD, Brown IWM, Kemmitt T, Bowden ME. Structural characterisation of heat-treated anodic alumina membranes prepared using a simplified fabrication process. J Membr Sci. 2007;287:264–70.
2. Vansant EF, Cool P. Chemical modifications of oxide surfaces. Colloid Surf A. 2001;179:145–50.
3. Tilley TD. Molecular design and synthesis of heterogeneous and single-site supported catalysts. J Mol Cat A Chem. 2002;182–183:17–24.
4. Shin E-J, Miser DE, Chan WG, Hajaligol MR. Catalytic cracking of catechols and hydroquinones in the presence of nano-particle iron oxide. Appl Cat B Environ. 2005;61:79–89.
5. Zhang Z, Hicks RW, Pauly TR, Pinnavaia TJ. Mesostructured forms of gamma alumina. J Am Chem Soc. 2002;124:1592–3.
6. Shi Q, Liang H, Feng D, Wang J, Stucky GD. Porous carbon and carbon/metal oxide microbers with well-controlled pore structure and interface. J Am Chem Soc. 2008;130:5034–5.
7. Flammea KEL, Popatb KC, Leonic L, Markiewiczc E, Tempad TJL, Romanc BB, Grimesd CA, Desaia TA. Biocompatibility of nanoporous alumina membranes for immunoisolation. Biomaterials. 2007;28:2638–45.
8. Popat KC, Swana EE, Mukhatyara V, Chatvanichkul K-I, Mor GK, Grimes CA, Desai TA. Influence of nanoporous alumina membranes on long-term osteoblast response. Biomaterials. 2005;26:4516–22.
9. Castner DG, Ratner BD. Biomedical surface science: foundations to frontiers. Surf Sci. 2002;500:28–60.
10. Jones FH. Teeth and bones: applications of surface science to dental materials and related biomaterials. Surf Sci Rep. 2001;42:75–205.
11. Greil PJ. Biomorphous ceramics from lignocellulosics. Eur Ceram Soc. 2001;21:105–18.
12. Ignjatovic N, Uskokovic D, Mihailova K.Synthesis and application of hydroxyapatite/polylactide composite biomaterial. Appl Surf Sci. 2004;238:314–19.
13. Advinculaa MC, Rahemtullaa FG, Advinculac RC, Adae ET, Lemonsa JE, Bellisa SL. Osteoblast adhesion and matrix mineralization on solgel-derived titanium oxide. Biomaterials. 2006;27:2201–12.
14. Qi X, Osterloh FE. Chemical sensing with $LiMo_3Se_3$ nanowire films. J Am Chem Soc. 2005;127:7666–7.
15. Dillon A, Mahan A, Deshpande R, Alleman J, Blackburn J, Parillia P, Heben M, Engtrakul C, Gilbert K, Jones K, To R, Lee S-H, Lehman J. Hot-wire chemical vapor synthesis for a variety of nano-materials with novel applications. Thin Solid Films. 2006;501:216–20.
16. Ionescu R, Espinosa E, Leghrib R, Felten A, Pireaux J, Erni R, Tendeloo GV, Bittencourt C, Canellas N, Llobet E. Novel hybrid materials for gas sensing applications made of metal-decorated MWCNTs dispersed on nano-particle metal oxides. Sens Actuators B Chem. 2008;131:174–82.
17. Gole JL, Lewis SE. Porous silicon and sensors and future applications. Nanosilicon 2008;4:149–75.
18. Long JW, Logan MS, Rhodes CP, Carpenter EE, Stroud RM, Rolison DR. Nanocrystalline iron oxide aerogels as mesoporous magnetic architectures. J Am Chem Soc. 2004;126:16879–89.
19. Schultz FS, Anderson MA. Effects of surface adsorption and confinement on thephotochemical selectivity of previtamin D3 adsorbed within porous sol-gel derived alumina. J Am Chem Soc. 1999;121:4933–40.
20. Vignes JL, Mazerolles L, Michel D. A novel method for preparing porous alumina objects. Key Eng Mater. 1997;132:432–5.
21. Pluedemann EP. Silane coupling agents. New York: Plenum Press; 1991.
22. Hair ML. Infrared spectroscopy in surface chemistry. London: Edward Arnold Publishers Ltd.; 1967.
23. Peri JB. A model for the surface of gamma alumina. J Phys Chem. 1965;69:220–30.
24. Knozinger H, Ratnasamy P. Catalytic aluminas: surface models and characterization of surface sites. Catal Rev. Sci Eng. 1978;17:31–70.
25. Tsyganenko AA, Mardilovich PP. Structure of alumina surfaces. J Chem Soc Faraday Trans. 1996;92:4843–52.
26. Morterra C. Proceedings of the 6th international Congress on catalysis, London 1976; 194.
27. Busca G, Lorenzelli V, Sanchez-Escribano V, Guidetti R. FT-IR study of the surface properties of the spinels $NiAl_2O_4$ and

$CoAl_2O_4$ in relation to those of transitional aluminas. J Catal. 1991;131:167–77.
28. Morterra C, Magnacca G. A case study: surface chemistry and surface structure ofcatalytic aluminas, as studied by vibrational spectroscopy of adsorbed species. Catal Today. 1996;27: 497–532.
29. Wislicenus H. Versuche zur Gerbstoffbestimmung ohne Hautpulver. Z Angew Chem. 1904;25:801–10.
30. Bennett J, Pinnel MJ. Reactions between mercury-wetted aluminium and liquid water. Mater Sci. 1973;8:1189–93.
31. Zhou RS, Snyder RL. Structures and transformation mechanisms of transition aluminas. Acta Crystallogr B Struct Sci. 1991;47: 617–30.
32. Van Santen RA. Theoretical heterogeneous catalysis. Singapore: World Scientific Publishing; 1991.
33. Flanigen EM, Khatami H, Syzmanski HA. Molecular sieve zeolites. Adv Chem Ser. 1971;16:201–28.
34. Aronne A, Esposito S, Pernice P. FTIR and DTA study of lanthanum aluminosilicate glasses. Mater Chem Phys. 1997;51: 163–8.
35. Aronne A, Esposito S, Ferone C, Pansini M, Pernice P. FTIR study of the thermal transformation of barium-exchanged zeolite A to celsian. J Mater Chem. 2002;12:3039–45.
36. Sitarz M, Mozgawa W, Handke M. Rings in the structure of silicate glasses. J Mol Struct. 1999;511:281–5.
37. Lutz W, Ruscher C, Heidemann, D. Determination of the framework and non-framework SiO_2 and AlO_2 species of steamed and leached faujasite type zeolites: calibration of IR, NMR, and XRD data by chemical methods. Microporous Mesoporous Mater. 2002;55:193–202.
38. Wang S, Dou T, Li Y, Zhang Y, Li X, Yan Z. Synthesis, characterization, andcatalytic properties of stable mesoporous molecular sieve MCM-41 prepared from zeolitemordenite. J Solid State Chem. 2004;177:4800–5.
39. Davydov AA. Infrared spectroscopy of adsorbed species on the surface of transition metal oxides. Chichester: Wiley; 1990.
40. Lamotte J, Moravek V, Bensitel M, Lavalley J. FT-IR study of the structure and reactivity of methoxy species on ThO_2 and CeO_2. React Kinet Catal Lett. 1988;36:113–18.
41. Jayasooriya UA, Anson C, Al-Joder O, dAlfonso G, Stanghellini P, Rossetti R. Vibrational assignments for methoxy ligands on metal clusters: interpretation of RAIRSdata from methoxy groups on single crystal copper surfaces. Surf Sci. 1993;294:131–40.
42. Dastoor H, Gardner P, King D. Identification of two tilted adsorbed methoxy specieson Ni(110) using RAIRS. Chem Phys Lett. 1993;209:493–8.
43. Montagne X, Lynch J, Freund E, Lamotte J, Lavalley J. A study of the adsorption sites on thoria by scanning transmission electron microscopy and Fourier-transform infrared spectroscopy. Adsorption and desorption of water and methanol. J Chem Soc Faraday Trans I. 1987;83:1417–25.
44. Nakamoto K. Infrared spectra of inorganic and coordination compounds. New York: Wiley; 1970.
45. Dyan A, Cenedese P, Dubot P. Physical properties of gamma alumina surface hydroxyls revisited through a large scale periodic quantum-chemistry approach. J Phys Chem B. 2006;20: 10041–50.
46. Dubot P, Cndse P. Modeling of molecular hydrogen and lithium adsorption on single-wall carbon nanotubes. Phys Rev B. 2001;63:241402(1)–(4).
47. Hoffmann R. Solids and surfaces. A chemists view of bonding in extended structures. New York: VHC Publishers, Inc.; 1988.
48. Little L. Infrared spectra of adsorbed species. London: Academic Press Inc.; 1966.
49. Barr TL. Recent advances in x-ray photoelectron spectroscopy studies of oxides. J Vac Sci Technol A. 1991;9:1793–806.